












Dithering-based real-time control of cascaded silicon photonic devices by means of non-invasive detectors

Francesco Zanetto¹  | Vittorio Grimaldi¹  | Fabio Toso¹  |
 Emanuele Guglielmi¹  | Maziyar Milanizadeh¹  | Douglas Aguiar¹  |
 Miltiadis Moralis-Pegios²  | Stelios Pitris²  | Theoni Alexoudi²  |
 Francesco Morichetti¹  | Andrea Melloni¹  | Giorgio Ferrari¹  | Marco Sampietro¹ 

¹Department of Electronics, Information and Bioengineering, Politecnico di Milano, Milano, Italy

²Department of Informatics, Center for Interdisciplinary Research and Innovation, Aristotle University of Thessaloniki, Thessaloniki, Greece

Correspondence

Francesco Zanetto, Department of Electronics, Information and Bioengineering, Politecnico di Milano, Piazza Leonardo da Vinci 32, Milano, 20133, Italy.

Email: francesco.zanetto@polimi.it

Funding information

H2020 Leadership in Enabling and Industrial Technologies, Grant/Award Number: 688172; H2020 Marie Skłodowska-Curie Actions, Grant/Award Number: 722779; H2020 Leadership in Enabling and Industrial Technologies, Grant/Award Number: 871658; H2020 Future and Emerging Technologies, Grant/Award Number: 829116

Abstract

Real-time control of multiple cascaded devices is a key requirement for the development of complex silicon photonic circuits performing new sophisticated optical functionalities. This article describes how the dithering technique can be leveraged in combination with non-invasive light probes to independently control the working point of many photonic components. The standard technique is extended by introducing the concept of orthogonal dithering signals to simultaneously discriminate the effect of different actuators, while the idea of frequency re-use is discussed to limit the complexity of control systems in cascaded architectures. After a careful analysis of the problem, the article presents an automated feedback strategy to tune and lock photonic devices in the maxima/minima of their transfer functions with given response speed and sensitivity. The trade-offs of this approach are discussed in detail to provide guidelines for the design of the feedback loop. Experimental demonstrations on a mesh of Mach-Zehnder interferometers and on cascaded ring resonators are discussed to validate the proposed control architecture in different scenarios and applications.

1 | INTRODUCTION

The high integration density made possible by silicon photonics enables the design of increasingly complex photonic architectures in a very small footprint, where a cascade of several devices is exploited to perform different optical functionalities like modulation, multiplexing and routing [1]. However, the increasing complexity of these systems revealed the difficulty of operating high-density architectures in an open-loop way because of their high sensitivity to fabrication parameters and temperature variations. A local monitoring of the working point of the most sensitive devices and the use of actuators to actively control them are consequently required to successfully operate complex structures.

Several algorithms and strategies have been indeed developed to tune, reconfigure and operate photonic systems even in the presence of thermal crosstalk, fabrication tolerances and unstable environmental conditions. To date, control techniques have already been demonstrated to drive trees of Mach-Zehnder interferometers (MZIs) [2,3], to control add-drop ring filters [4], to lock ring modulators [5] and many others. Most of the proposed control methods rely on the extraction and measurement of a small part of the light from the main optical path [6]. This solution becomes quickly unfeasible for high-density systems, where the insertion of many detectors causes an unacceptable drop of the overall optical power reaching the output. In some cases, light tapping can even impair the circuit functionality, like in mode-division-multiplexing based architectures [7].

This is an open access article under the terms of the Creative Commons Attribution License, which permits use, distribution and reproduction in any medium, provided the original work is properly cited.

© 2021 The Authors. *IET Optoelectronics* published by John Wiley & Sons Ltd on behalf of The Institution of Engineering and Technology.

An increasing research effort is thus being carried out to develop and use in-line non-invasive photodetectors, that promise to solve the aforementioned issues and allow the control of large-scale architectures [8]. In [9], the resonance stabilization of ring resonators was demonstrated using a transparent detector, that however uses an extra ion-implantation processing step to increase the sensitivity of the readout. In [10,11], the control of complex architectures is shown, exploiting the photoconductive effect of integrated waveguide heaters to sense light inside each photonic device. In addition to the excess losses caused by the required waveguide doping, a calibration of the control system was needed to account for the dark current of the detectors, a time and resource consuming approach that might become unpractical as the number of sensors increases.

A possible fully transparent in-line alternative to monitor the state of complex photonic circuits is the ContactLess Integrated Photonic Probe (CLIPP) [12], a detector that senses light in silicon waveguides just by exploiting their natural losses. Owing to phenomena like Surface-State absorption (SSA) [13], light in a silicon waveguide generates a small amount of free carriers, consequently changing the electrical conductivity of the core. By measuring the electrical impedance of a portion of a waveguide, it is thus possible to assess the local light intensity, relying exclusively on the natural propagation losses. The access to the electrical properties of the waveguide cannot be obtained by directly contacting the core, since this would cause additional optical losses, so a capacitive coupling is preferred, achieved by placing two metal electrodes on top of the cladding at around 700 nm from the core. This approach makes the fabrication of the sensor possible in any standard technology.

The use of CLIPP sensors has already been validated to operate complex photonic architectures [14–16], yet with a focus more on the final application than on a description of the control strategies. To fill this gap, this paper generalizes and extends to cascaded systems what is reported in [17] about the control of single devices. The stabilization of complex photonic architectures requires in fact additional strategies and techniques to take into account the reciprocal coupling and interaction between stages while avoiding calibration procedures, that are unpractical for large-scale systems. To this aim, the opportunity given by the CLIPP to monitor in principle any point of a complex photonic network finds its perfect match with the dithering technique. In this work, the standard technique is extended by introducing the concept of orthogonal dithering signals for the discrimination of multiple actuators, while the idea of frequency re-use is presented as an effective way to limit the complexity of control systems. These strategies allow to independently address each photonic device and track variations of the working conditions without requiring any calibration, making them suitable for high-density architectures where a high number of sensors and control loops are needed.

The article is organized as follows: Section 2 provides a close look to the dithering technique, showing how it can be extended and used in combination with CLIPP detectors. In Section 3, the implementation of a calibration-free automated control loop is presented, exploiting integral controllers to close a real-time feedback and stabilize the working point of

photonic devices. Several experimental results confirm the effectiveness of the proposed approach. A concluding section summarizes the main findings of the paper.

2 | LOCKING A PHOTONIC DEVICE: THE DITHERING TECHNIQUE

Many complex photonic architectures rely on the use of a cascade of resonant or interferometric devices to guide light along a certain path and obtain the desired optical functionality. These devices are usually tuned to maximize or minimize the amount of light that reaches one of their outputs, in order to completely steer it from one waveguide to another. This working point needs to be stabilized against fluctuations of both temperature and wavelength, that are unavoidable in realistic environments and might impair the functionality of the system. Several locking techniques have been proposed in literature to stabilize the operation of photonic devices, for instance by monitoring the output power level [18] or the bit-error rate of optical signals [19]. However, these strategies are not convenient in cascaded photonic systems, where the change of optical power measured after a certain device can be the consequence of something happening upstream. In addition, by monitoring these parameters around the maximum (or minimum) of a transfer function, it is difficult to understand in which direction the optimal working point shifts as consequence of thermal or wavelength variations, due to the symmetry of many photonic devices.

A very effective way to implement power independent tuning and control algorithms is the dithering technique [20]. The technique allows to extract in real-time the derivative of the transfer function of an optical device directly from the physical system and this information can be effectively exploited to tune and stabilize its working point. Indeed, the power emerging from a photonic device can be maximized (or minimized) by driving to zero the output dithering signal, since this condition indicates stationary points of the transfer function. This approach is suitable for cascaded architectures, because the set-point does not require any calibration and does not depend on the absolute amount of light that reaches a device. In addition, in case of variations of the optimal working point, it is possible to understand the direction of the shift from the sign of the derivative, leaving no ambiguity on the control action to be taken. Finally, variations of the dark readout baseline do not affect the measurement, allowing to effectively use the dithering readout as error signal of a robust closed-loop control system. The main drawback of this approach is that, to perform the extraction of the derivative information, only a small fraction of the optical signal reaching a sensor is exploited. Consequently, to obtain a proper sensitivity in the detection of light and efficiently use the dithering information for control purposes, a narrow readout bandwidth is usually required. The speed of a dithering-based system might thus be slower than the other implementations mentioned before. A more complex lock-in based electronics is

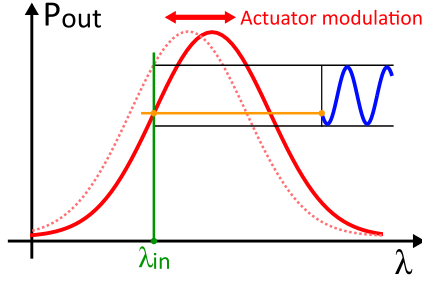


FIGURE 1 Working principle of the dithering technique. By driving an actuator with a modulated signal, an oscillation of the transfer function is produced around its bias point, leading to an output amplitude modulation of the optical power

also required to extract the dithering information from the sensor readout, as explained in the following section.

2.1 | Modulation signal and lock-in extraction

In order to extract the transfer function derivative, a small modulation signal is superimposed to the actuator voltage that controls the optical device of interest, causing an oscillation of the transfer function around its bias working point and a consequent modulation of the optical power at the output, as depicted in Figure 1. Any periodic waveform can be used to modulate the actuator voltage. If the dithering signal is sufficiently small (typically from few millivolts when controlling ring resonators up to some tens of millivolts in case of MZIs, on top of a bias of few volts), the amplitude of the output power modulation is directly proportional to the slope of the transfer function, that is to its first derivative, around the bias point. Indeed, considering a sinusoidal dithering:

$$V_{ACT}(t) = V_{BIAS} + v_{dith} \sin(2\pi f_{dith} \cdot t)$$

If $v_{dith} \ll V_{BIAS}$ (condition met in most of the cases), the output power can be approximated as:

$$P_{OUT}(t) \approx P_{OUT}(V_{BIAS}) + P_{dith} \sin(2\pi f_{dith} \cdot t) \quad (1)$$

where

$$P_{dith} = v_{dith} \cdot \left. \frac{\partial P_{OUT}}{\partial V_{ACT}} \right|_{V_{ACT}=V_{BIAS}} \quad (2)$$

and V_{ACT} is the driving voltage of the actuator, V_{BIAS} the initial bias voltage, v_{dith} and f_{dith} the amplitude and the frequency of the dithering signal, respectively.

The extraction of the dithering information can be obtained by placing a CLIPP detector directly at the output of the photonic device, operating it with a lock-in technique. The sensor readout will in fact contain both the DC information

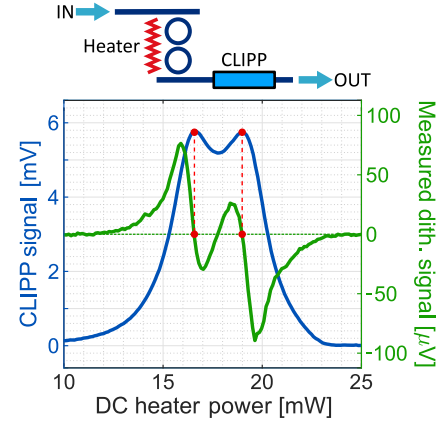


FIGURE 2 Transfer function (blue) and output dithering signal (green) of a double-ring resonator filter, experimentally measured with a CLIPP. As expected, the stationary points of the transfer function correspond to the zero crossings of the dithering signal

because of the average power and a modulated contribution at f_{dith} . This dithering fraction can be conveniently isolated and extracted with a lock-in processing. With respect to other implementations, like peak-stretchers or envelope detectors, the lock-in technique has the advantage of being frequency and phase selective, thus allowing to isolate and extract only the useful information and reject spurs and disturbs. In addition, the mixing action of the lock-in has the beneficial effect of upconverting the $1/f$ noise of the readout chain to high frequency, allowing to extract the small dithering signal with the highest resolution possible.

Equation (2) shows that the output modulation P_{dith} is proportional to both the dithering amplitude v_{dith} and the transfer function derivative. To maximize the readout signal, it is then possible to increase the dithering amplitude. However, depending on the application, a large modulation may disturb the operation of the optical device under test. Therefore, the amplitude of the dithering sinusoid must be chosen carefully, evaluating the trade-off between a higher signal-to-noise ratio (SNR) and the perturbation of the optical functionality [20]. It should be noticed that, when a stationary point is reached, the residual perturbation is minimized, being the transfer function flat in that region. Therefore, when locking to the maximum or minimum of a transfer function, a larger dithering signal is usually allowed, as compared to other working points. Although it might increase the complexity of the system, adaptive dithering amplitude could be envisioned for optimum results. Notice also that the amplitude of the modulation signal should be smaller than the minimum detail of the transfer function of interest: a device with multiple maxima and minima requires for instance an amplitude small enough to observe a response related to the single peaks. Figure 2 shows an experimental example of CLIPP-measured transfer function (obtained by subtracting the dark baseline from the readout) and output dithering signal of a cascaded double-ring filter. The dithering amplitude was limited to 10 mV, corresponding to around 300 μ W in terms of power, to observe both the resonance peaks. It is possible to see that, as expected, the two

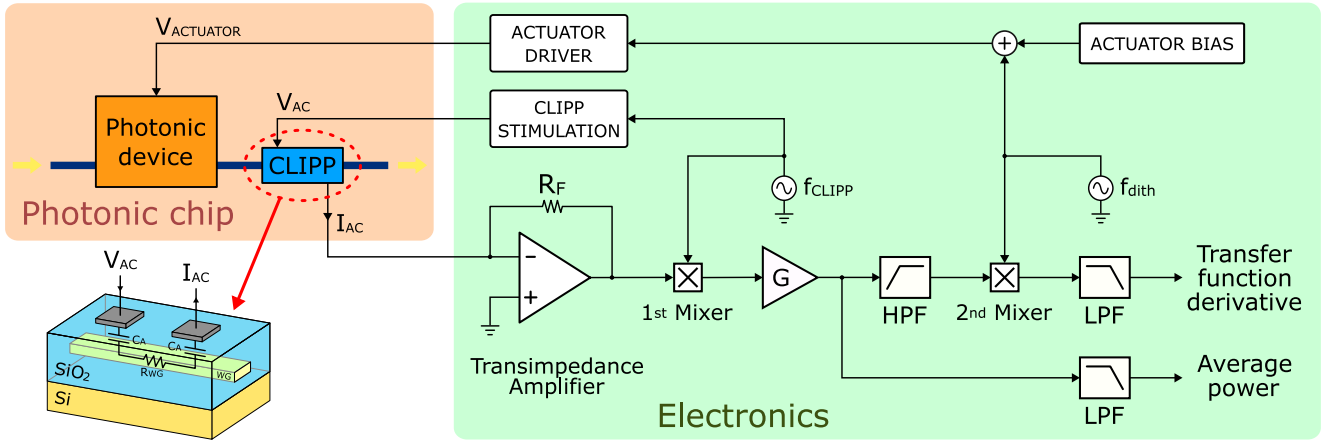


FIGURE 3 Schematic of the two-stage lock-in readout used to extract both the average power information and the dithering information with CLIPP detectors. The 3D model of the sensor is also reported

maxima of the transfer function correspond to the zero crossing points of the dithering readout.

2.2 | Dithering readout with CLIPP detectors

When using a CLIPP detector, the lock-in processing should take into account the AC coupled mode of operation of the sensor (because of its contactless nature) and the frequency spectrum of its electrical response. Figure 3 shows a 3D representation of the CLIPP sensor and its simplified equivalent electrical model, neglecting the effect of the substrate and of the coupling between the electrodes [21]. In order to bypass the access capacitance C_A and probe the electrical resistance of the core R_{WG} , one pad of the sensor must be stimulated at a frequency $f_{CLIPP} \gg 1/2\pi C_A R_{WG}$, usually between 100 kHz and 10 MHz, depending on the geometry of the electrodes and the photonic technology used. The other pad, connected to the virtual ground of a TransImpedance Amplifier (TIA), is used to collect the current coming from the sensor and convert it into a voltage. The amplitude of the signal at f_{CLIPP} allows to infer the waveguide resistance R_{WG} and therefore the local optical power.

When the dithering technique is used, due to the sinusoidal stimulation of the sensor, the modulated signal at f_{dith} is upconverted at f_{CLIPP} . To recover the dithering information, a two-stage lock-in technique is thus needed, as shown in Figure 3. A first mixer is used to demodulate the CLIPP signal at f_{CLIPP} , thus downconverting the information of the average optical power to DC and the dithering signal back to low frequency. After amplification and AC coupling, a second mixer, fed with the same signal at f_{dith} used to generate the dithering modulation, extracts the derivative information. The two-stage lock-in processing is finally completed by a low-pass filter, that removes the residual high frequency replicas generated by the mixing action and sets the overall bandwidth of the measurement according to the well-known trade-off between sensitivity and response time (see also Section 3.3).

2.3 | Orthogonal dithering for discrimination of multiple actuators

The dithering technique can be effectively used also to discriminate the effect of multiple actuators, while still using only a single detector. This feature is very useful in case of devices that require more than one heater to be operated, like MZIs, or in cascaded structures where many actuators affect the output optical power, like arrays of coupled microring resonators. In these situations, operating by only looking at the average output power requires complex techniques to take into account thermal crosstalk effects and perform an effective tuning action [22].

The orthogonality principle can be instead leveraged to easily separate the contribution of each actuator when using the dithering technique. Recalling that:

$$\sin(2\pi f_1 t) \perp \sin(2\pi f_2 t) \text{ if } f_1 \neq f_2 \quad (3)$$

by applying to the actuator modulations at different frequencies, each dithering signal can be independently recovered from the lock-in based sensor readout. Indeed, by simultaneously demodulating the CLIPP output at the different frequencies, each dithering can be extracted in parallel, to have the information of the effect of all the actuators at the same time. Notice that some residual crosstalk can arise because of the spurious harmonics produced either by the dithering generator or by the non-linearities of the photonic device transfer function. This effect can be completely suppressed by choosing the dithering signals at non-harmonic frequencies, like for instance 5, 7, 9 and 11 kHz. The phase selectivity of the lock-in technique can also be exploited to use couples of dithering signals at the same frequency, but in quadrature with each other. In this way, the number of frequencies to be generated in case of complex structures can be halved.

An experimental demonstration of this principle was carried out on a MZI featuring two heaters, as shown in Figure 4a. The use of two heaters in a single MZI is useful to

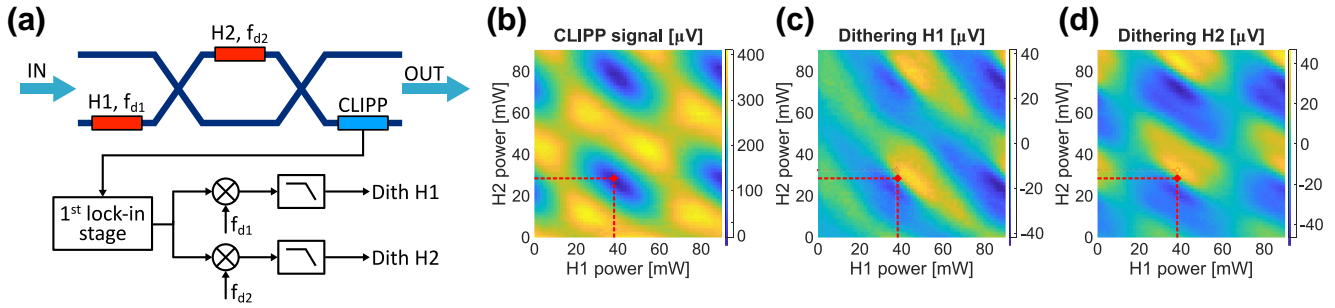


FIGURE 4 (a) Mach-Zehnder interferometer control scheme when using two heaters with orthogonal dithering signals. (b) Colour map of the MZI transfer function obtained with a CLIPP detector at the lower output branch. (c), (d) Partial derivatives of the MZI transfer function, extracted in parallel by using orthogonal dithering signals. The three maps, made of 60×60 points, were obtained simultaneously with an acquisition time of 5 ms per pixel

implement an amplitude-and-phase tunable coupler, needed in structures like the one presented in Section 3.2. A continuous-wave (CW) laser at 1550 nm was split and launched to both inputs of the MZI to perform the experiment. The voltage of the heaters was scanned from 0 to 6 V to obtain a map of the output light, measured with a CLIPP for each combination of heater powers, as shown in Figure 4b. Two dithering signals of 50 mV amplitude at 5 and 7 kHz, respectively, were applied to the heaters and the CLIPP readout was demodulated in parallel at the two frequencies to extract the partial derivatives of the output power. Figure 4c,d show the obtained result. The system was able to correctly discriminate the effect of the two actuators and recover the information. The optimal working point to completely steer light on one of the output branches (red dot in Figure 4b–d) can now be easily found by applying to the heaters the combination of voltages that drives to zero both dithering signals with two simple and completely independent control loops, as discussed in Section 3.

2.4 | Dithering frequency re-use in cascaded systems

Cascaded systems take particular profit of the dithering technique, as the use of orthogonal modulations can be exploited to address each device independently using a limited number of sensors, making the control strategy insensitive to reciprocal coupling. However, the generation and processing of many orthogonal modulations becomes rapidly unfeasible as the complexity of the system increases. The possibility to use the same dithering signals multiple times is very beneficial to simplify the control architecture in these situations. The peculiar nature of cascaded photonic systems helps to achieve this goal: their tuning procedure is in fact inherently sequential, as one stage can be completely configured only when the previous one has reached its final working point. This mode of operation makes it possible to recycle dithering signals.

As already mentioned, when a photonic device is configured to work in a stationary point, the residual dithering modulation that survives at its output is minimized, thanks to the transfer function flatness in this region. In addition, since photonic devices are normally symmetric around their

maxima/minima, the frequency of the residual oscillation is doubled with respect to the dithering one. These two properties can be exploited to control cascaded architectures using the same modulation for all the optical devices, as they guarantee that ideally no interaction is observed when the equilibrium condition is reached. The interaction between stages is indeed only happening during an initial transitory phase but it is not a problem for the operation of the photonic architecture since it does not prevent to reach the correct working point.

The configuration of a cascaded architecture, obtained with a single dithering frequency, thus works in a sequential way. The first stage, whose output contains only the information of its own dithering, can be configured immediately. While this tuning is in progress, the downstream stages receive an optical signal also containing the modulation of the first device, so they cannot correctly complete their configuration. When the first stage is set, the residual dithering oscillation at its output is minimized, so the second device can be tuned correctly. All the stages can be thus sequentially controlled until the full architecture is configured, making this procedure well suited for cascaded systems. An experimental demonstration of this working principle is shown in Section 3.2.

In real operations a small interaction between stages might survive due to offsets and non-idealities, but its impact is usually negligible. The residual modulation of a stage gets attenuated by each device it passes through, so crosstalk effects are observed almost only between consecutive stages. In order to minimize this issue, a couple of orthogonal dithering signals can be used, rotating them every two devices. In this way, optimal operation is still possible while keeping the complexity of the system reasonably low.

3 | DITHERING-BASED AUTOMATED CONTROL ARCHITECTURE

Locking the working point of a device to the maximum/minimum of its transfer function requires driving the dithering readout to zero. Several approaches can be used to minimize a signal, like stepper or gradient descent algorithms [23,24]. The use of an integral controller is here presented and discussed. With respect to other techniques, an integral controller can be

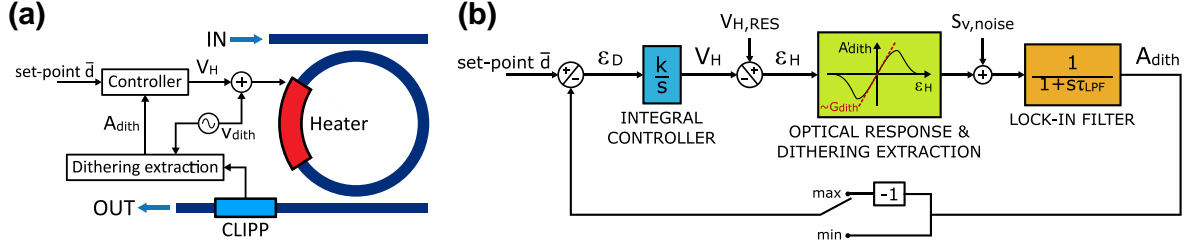


FIGURE 5 (a) Example of CLIPP-based control scheme applied to a microring resonator. (b) Block diagram of the closed-loop architecture that can be implemented to lock the working point of photonic devices, based on the dithering technique and an integral controller

easily implemented both in digital and analogue systems. In the following, its closed loop behaviour is conveniently studied in the continuous-time domain.

3.1 | Integral controller

As an example of general validity, let us consider the locking of a microring resonator obtained by means of a thermal actuator and a CLIPP detector, as shown in Figure 5a. The schematic block diagram of the proposed control system is reported in Figure 5b. The ring resonator is characterized by a heater voltage $V_{H,RES}(\lambda, T)$ that drives it at resonance. Notice that $V_{H,RES}$ is a function of the wavelength λ and of the instantaneous temperature of the system T and as such it changes during the operation of the photonic device. The role of the control loop is to track the variations of $V_{H,RES}$ in real-time and apply to the heater the correct voltage V_H that matches $V_{H,RES}$. The system exploits the extracted dithering amplitude A_{dith} to monitor the microring working point, so the input and set point of the feedback loop is the desired derivative value \bar{d} to be reached at the equilibrium. The value of \bar{d} can be tuned to lock any arbitrary working condition and it is set to zero when a stationary point is targeted. The system works to drive the error signal $\epsilon_D = \bar{d} - A_{dith}$ to zero, in order to keep the value of A_{dith} equal to the set-point.

Depending on the instantaneous difference ϵ_H between the target value $V_{H,RES}$ and the actual heater voltage V_H , a certain amount of light circulates in the ring resonator and it is measured by the CLIPP sensor. As discussed in Section 2.2, the CLIPP signal is detected, after amplification, with the lock-in technique to extract the dithering information. Consequently, the sensor readout can be described with the *optical response and dithering extraction* block, that relates the heater detuning ϵ_H to the measured dithering amplitude A_{dith} , and with a low-pass filter having a transfer function $1/(1 + s\tau_{LPF})$, where τ_{LPF} is the time constant of the second lock-in stage. The filter is needed to remove the harmonics resulting from the dithering demodulation, that would otherwise impair the loop functionality. Although the relation between heater voltage and measured dithering amplitude is generally described by a non-linear function, for simplicity here we assume the case of small perturbations around resonance, where a linearized model can be used. In this case, the *optical response and dithering extraction* block can be simplified and

considered as a constant gain G_{dith} , representing the slope of the curve around resonance. An inverting stage can be used to change the sign of the acquired dithering amplitude A_{dith} , to be able to lock both maxima and minima of the transfer function of interest, depending on the requirement of the application. An integral controller, with transfer function k/s , completes the feedback loop. The parameter k defines the gain of the controller and can be tuned to ensure the stability of the system.

Based on this discussion, the loop gain G_{loop} of the system and the error signal ϵ_D can be computed as:

$$G_{loop}(s) = -\frac{G_{dith}}{1 + s\tau_{LPF}} \cdot \frac{k}{s} \quad (4)$$

$$\epsilon_D(s) = \frac{\bar{d}(s)}{1 - G_{loop}} - \frac{V_{H,RES}(s) \cdot G_{dith}}{1 + s\tau_{LPF}} \cdot \frac{1}{1 - G_{loop}} \quad (5)$$

The qualitative Bode plot of the loop gain is shown in Figure 6a. Assuming that the Bode criterion is satisfied to guarantee the stability of the system, that is the sensor readout pole $f_{LPF} = 1/2\pi\tau_{LPF}$ is correctly placed after the zero-crossing point of the loop gain, the closed-loop bandwidth of system can be computed by solving for $|G_{loop}| = 1$:

$$BW_{CL} = \frac{G_{dith} \cdot k}{2\pi} \quad (6)$$

This bandwidth, that can be tuned by choosing the value of k , defines the maximum frequency at which the feedback loop can react to variations of the ring resonance voltage and minimize the error signal. This can also be observed by looking at the expression of ϵ_D , at frequencies below the lock-in readout pole, when \bar{d} is set to zero:

$$\epsilon_D(s) \approx -\frac{V_{H,RES}(s)}{k} \cdot \frac{s}{1 + \frac{s}{G_{dith} \cdot k}} \quad (7)$$

The qualitative Bode plot is reported in Figure 6b. A high-pass action is clearly visible, meaning that, within the feedback bandwidth, the loop works to minimize the error signal, thus keeping the extracted derivative A_{dith} equal to zero and

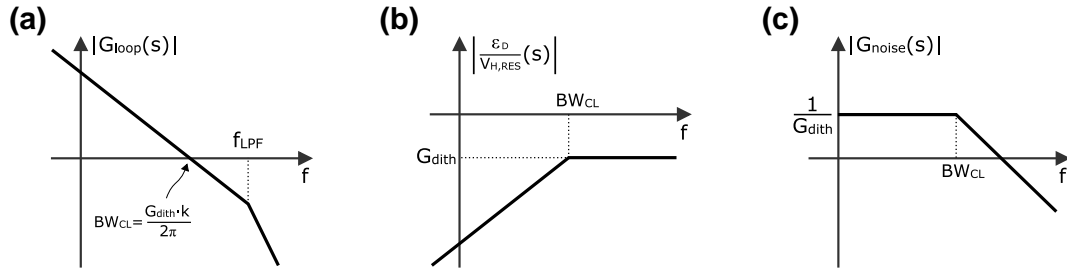


FIGURE 6 Qualitative Bode plots of the (a) loop gain, (b) error signal and (c) noise transfer function obtained when the control scheme of Figure 5 is used to stabilize photonic devices

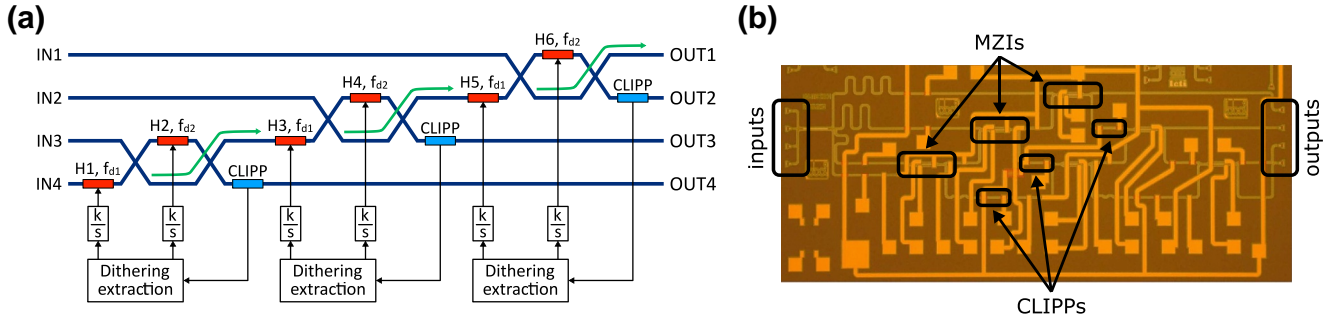


FIGURE 7 (a) Schematic of the MZI based self-aligning beam coupler. The six parallel control loops needed to control the architecture are also reported. (b) Micro-photograph of the chip fabricated in a commercial silicon photonics platform, with a footprint of 3.7×1.5 mm

consequently the ring at resonance. As the frequency increases, the loop cannot react any more to variations of the ring working point and the error signal starts to follow $V_{H,RES}$. This behaviour confirms that the proposed control strategy can be effectively exploited to lock the resonance of photonic devices against fluctuations within the feedback bandwidth. By changing the value of the integral controller gain k , it is possible to tune the bandwidth of the control loop to satisfy the requirements of the application. The upper limit of the bandwidth is determined by two factors: the stability of the feedback loop must be guaranteed and the actuation noise resulting from the control action should be kept sufficiently low. Indeed, a larger bandwidth also implies higher actuation noise (as explained in Section 3.3), so k should be tuned to achieve a sufficiently fast response without introducing too much noise, that would degrade the accuracy of the locking action.

3.2 | Experimental demonstration

The proposed control architecture was experimentally tested in the complex photonic system shown in Figure 7a. The circuit is a self-aligning beam coupler, made of a mesh of three cascaded MZIs, that can detect and compensate the phase difference of the light arriving to its inputs, to collect and extract it from a single output [25]. Figure 7b shows the micro-photograph of the chip, fabricated in a commercial silicon photonics platform. Each interferometer is controlled by means of two heaters and a CLIPP on the lower output branch, as previously reported in

Figure 4. The partial derivatives of the MZIs, extracted with the dithering technique, are fed to a set of digital integral controllers [26], operating in parallel to drive the dithering signals to zero. Six independent feedback loops are thus needed to control the full architecture. In order to limit the number of dithering signals to be generated, the working principle of Section 2.4 can be exploited: thanks to the ideally null residual oscillation that survives after each stage when the locked condition is reached, the full mesh can be configured by only using two dithering frequencies. Indeed, all the MZIs were controlled with the same orthogonal modulations with 50 mV amplitude at 5 and 7 kHz, respectively.

To test the control architecture, a CW laser at 1550 nm was split and injected to the photonic circuit, with a power of around 0 dBm reaching each input. The power at OUT1 was monitored with an external bench-top photodiode (PD), to provide a standard reference measurement. The voltages of the heaters were set to random initial values and after 5 ms the control loops were activated. Figure 8a shows the configuration transients of a single MZI and of the full mesh acquired by the PD, for two different values of the control loop bandwidth. It is possible to notice that the transients of the single MZI are exponential, coherently with what expected when using an integral controller. Figure 8b reports the theoretical configuration time of a single MZI as a function of the control bandwidth, obtained by considering five time constants τ of the closed-loop system ($\tau = 1/2\pi BW_{CL}$, in Equation (6) $G_{dith} = 275 \mu\text{V/V}$, $k = 2.3 \times 10^5$, 4.6×10^5 , 9.2×10^5 , 18.4×10^5 respectively). The curve shows very good agreement with the experimental measurements, that were repeated

20 times for each bandwidth from different initial heater voltages to obtain relevant statistics. A maximum bandwidth of 80 Hz was found to be a good compromise between response time (down to 12 ms) and accuracy of the locking procedure in these experimental conditions.

When moving from a single MZI to the full mesh, a sequential tuning of the interferometers is inherently required, even when using parallel control loops, as the phase difference between the inputs of each MZI depends on the configuration of the previous stages. This causes an increase of the overall tuning time with respect to the single MZI, as it can be observed in Figure 8a. The transient is also no longer exponential, since in this situation the output is the result of a cascade of three devices. Nevertheless, the control system was able to configure the full mesh in down to 20 ms when selecting a bandwidth of 80 Hz. Interestingly, a penalty factor of just 1.6 was observed when passing from a single MZI to a mesh of three devices (Figure 8c), suggesting that, even if frequency re-use was exploited, thanks to the parallel control loops the configuration of a MZI could start slightly before the complete setup of the previous one. Again, the experiment was repeated 20 times for each bandwidth from random initial heater voltages to test the robustness of the feedback. Convergence was achieved in all cases with statistics similar to the single MZI case, as proof of the correct design and operation of the architecture in routing all the light to the correct output.

3.3 | Noise versus bandwidth trade-off

In order to quantify the relation between the bandwidth of the control loop and the residual noise, the transfer function from readout noise $S_{v,noise}$ to actuation voltage V_H of the general architecture can be computed. From Figure 5, it is:

$$G_{noise}(s) = \frac{k}{s} \cdot \frac{1}{1 - G_{loop}} \approx \frac{1}{G_{dith}} \cdot \frac{1}{1 + \frac{s}{G_{dith} \cdot k}} \quad (8)$$

The readout noise is here considered as the main noise source and it is modelled with a voltage generator placed after the dithering readout block, since in the real system it is superimposed to the extracted dithering signal. A qualitative Bode plot of the noise transfer function is reported in Figure 6c. It is possible to observe that the noise of the readout is transferred to the actuation voltage for frequencies up to BW_{CL} and then low-pass filtered. Consequently, the RMS noise that affects the actuation voltage for a given bandwidth can be computed as:

$$\begin{aligned} V_{H,noise} &= \sqrt{S_{v,noise}} \cdot \frac{1}{G_{dith}} \cdot \sqrt{\frac{\pi}{2} \cdot BW_{CL}} = \\ &= \sqrt{S_{v,noise}} \cdot \sqrt{\frac{k}{4 \cdot G_{dith}}} \end{aligned} \quad (9)$$

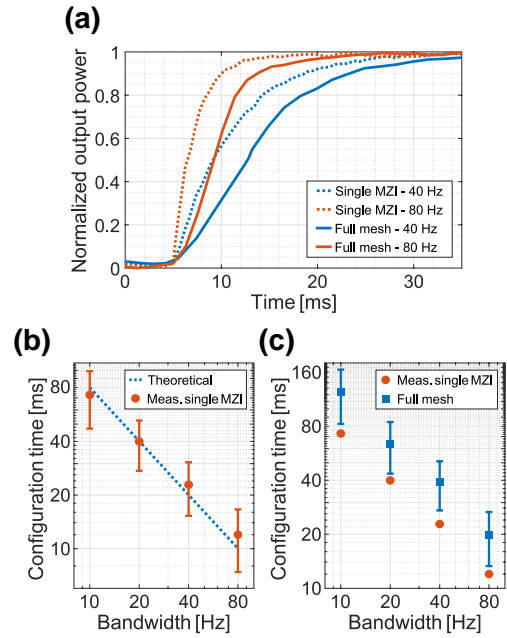


FIGURE 8 (a) Experimentally measured configuration transients of a single MZI and of the full mesh, for two different control loop bandwidths. (b) Configuration time of a single MZI as function of the control bandwidth, showing very good agreement with the theoretical values predicted by Equation (6). (c) Configuration time of the full mesh, achieved with a penalty of only a factor 1.6 when compared to the single MZI case

where $S_{v,noise}$ is the voltage noise power spectral density of the readout. Notice that this computation is true only if $S_{v,noise}$ can be considered as white noise. This is indeed our case, since the $1/f$ noise is removed thanks to the use of the lock-in technique. Since the factor G_{dith} is a parameter that cannot be controlled and assuming that $S_{v,noise}$ has already been minimized with proper electronic design, the only parameter that can be tuned to obtain the desired noise level is k , that also affects the control-loop bandwidth (Equation (6)). A lower k provides lower actuation noise and consequently a more accurate locking action, with the drawback of a lower control bandwidth. The choice of k is therefore the result of a careful trade-off between noise and speed of response and must be tuned depending on the requirements of the application. Notice that a noise reduction of a factor x is obtained at the price of a bandwidth narrowing of a factor x^2 .

3.4 | BER versus bandwidth measurement

To test the effect of the actuation noise on the locking accuracy, an experiment was performed on the photonic chip shown in Figure 9a. The circuit is an O-band routing engine, that features two cascaded double-ring filters to route light to one of the three outputs depending on its configuration. The transfer function of the two filters is the one previously shown in Figure 2, with a free spectral range of 9.6 nm and a bandwidth of 50 GHz. The locking of the two devices was implemented with two parallel control loops, using two dithering

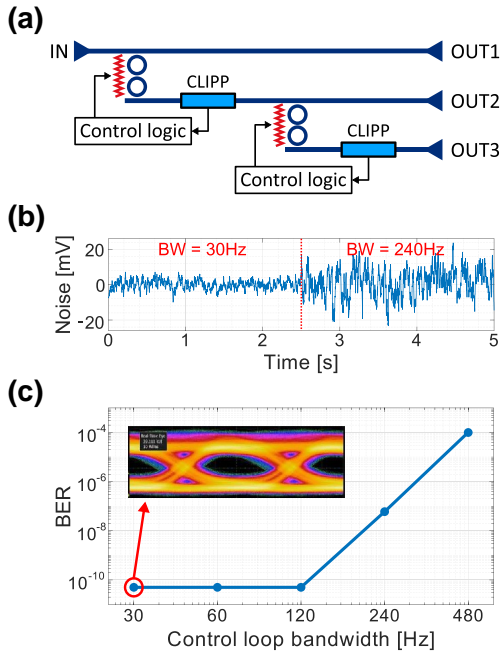


FIGURE 9 (a) Schematic of a microring resonator based O-band routing engine, with the corresponding control architecture. (b) Measured actuation noise in case of two different control bandwidths (30 Hz and 240 Hz). (c) Experimental BER measurement at OUT3 as a function of the control loop bandwidth. The inset of the figure reports the output eye diagram in case of a 30 Hz bandwidth

signals of 10 mV amplitude ($300 \mu\text{W}$ in terms of power) at 5 and 7 kHz, respectively, to align both filters to the input laser, thus maximizing the power at OUT3. A laser source at 1310 nm was modulated with a 30 Gbit/s NRZ signal by means of an external commercial MZI modulator, amplified and then coupled to the photonic chip, with an input power of 5 dBm. The output of the photonic circuit was monitored using a bit-error-rate (BER) tester, performing a 30 s cumulative BER measurement for each control bandwidth.

Figure 9b shows the time evolution of the actuation noise measured for two different values of the control bandwidth (30 and 240 Hz, respectively). As predicted by Equation (9), a noise increase is observed when a larger bandwidth is chosen. The equation is validated by the noise RMS values computed in the two conditions, that result to be 2.6 and 7.5 mV, respectively. The measured worsening factor is very close to the theoretical value of $\sqrt{8}$ predicted by the equation and dictated by the bandwidth increase, confirming the correctness of the previous discussion.

The quality of the optical transmission was monitored with the BER tester to assess the impact on the actuation noise on the optical functionality. The result is shown in Figure 9c. The system was able to ensure error-free transmission with BER of 5×10^{-11} for bandwidths up to 120 Hz, thanks to the low-noise readout implemented with the lock-in technique. The control loop was thus able to react to variations of the input

with a response time of around 6 ms with no penalty on the transmission. When further increasing the bandwidth, the actuation noise started to have a non-negligible effect. Indeed, a bandwidth of 240 Hz caused a small BER degradation, though still guaranteeing a good transmission. It was observed that, due to the increased noise level, the performance worsening was the consequence of an oscillation of the locking set-point between the two maxima of the coupled-ring filters (Figure 2). However, the resonance of the two devices was still preserved, allowing to correctly route light through them. A further increase of bandwidth to 480 Hz was instead not possible, because in these conditions the system was not able to lock the resonances. Recalling Equation (9), the only way to improve this limit is to increase the parameter G_{dith} , in order to increase the gain of the integral controller k without introducing additional noise. This can be obtained only by increasing the dithering amplitude, but the impact on the optical transmission must be evaluated to be sure not to degrade the functionality of the system. With the chosen 10 mV amplitude, the signal transmission was not affected, as it can be seen from the clearly open eye diagram in the inset of Figure 9c.

4 | CONCLUSIONS

This work presented and discussed how to reliably operate complex silicon photonic architectures made of many cascaded devices through the implementation of robust feedback control strategies. To guarantee scalability to the system, the non-invasive nature of CLIPP detectors was exploited to monitor multiple photonic devices simultaneously without impairing the overall optical functionality. The advantages of the dithering technique were fully exploited by implementing orthogonal modulations to discriminate the effect of different actuators, while frequency re-use allowed to keep the complexity of the control system low even when controlling many devices simultaneously.

The effectiveness of the control system was demonstrated on the configuration and locking of a mesh of three cascaded MZIs, achieved in down to 20 ms, thanks to six parallel integral control loops with a penalty of only a factor 1.6 with respect to the case of a single MZI. A second experimental result demonstrated error-free routing and transmission of a 30 Gbit/s optical signal through a cascade of microring resonator filters with a response time down to 6 ms (120 Hz bandwidth) at 5×10^{-11} BER, achieved, thanks to the low-noise lock-in elaboration of the signals.

Robust calibration-free control strategies are an essential milestone to support the development and real-life diffusion of increasingly complex photonic systems, that cannot be operated in an open-loop way due to unavoidable fluctuations of their optimal working point. Our approach overcomes the limitations of conventional invasive detectors and of calibration processes, enabling the design of architectures performing new optical and computational functionalities.

ACKNOWLEDGEMENTS

This work was supported by the EU H2020 projects ICT-STREAMS (grant no. 688,172), TRAINING4CRM (grant no. 722,779), NEBULA (grant no. 871,658) and Super-Pixels (grant no. 829,116).

We thank the staff of POLIFAB, the microelectronic facility of Politecnico di Milano, for their support in mounting the photonic chip.

ORCID

Francesco Zanetto  <https://orcid.org/0000-0002-0242-5016>

Vittorio Grimaldi  <https://orcid.org/0000-0003-1593-6103>

Fabio Toso  <https://orcid.org/0000-0001-7579-4552>

Emanuele Guglielmi  <https://orcid.org/0000-0003-4037-4755>

Maziyar Milanizadeh  <https://orcid.org/0000-0001-6568-7219>

Douglas Aguiar  <https://orcid.org/0000-0001-9237-1287>

Miltiadis Moralis-Pegios  <https://orcid.org/0000-0002-9401-730X>

Stelios Pitris  <https://orcid.org/0000-0001-5010-8843>

Theoni Alexoudi  <https://orcid.org/0000-0001-6722-201X>

Francesco Morichetti  <https://orcid.org/0000-0002-5858-2811>

Andrea Melloni  <https://orcid.org/0000-0002-6015-3290>

Giorgio Ferrari  <https://orcid.org/0000-0002-2854-8444>

Marco Sampietro  <https://orcid.org/0000-0003-4825-9612>

REFERENCES

- Moralis-Pegios, M., et al.: 4-channel 200 Gb/s WDM O-band silicon photonic transceiver sub-assembly. *Optic. Express.* 28(4), 5706–5714 (2020)
- Mak, J.C.C., Poon, J.K.S.: Multivariable tuning control of photonic integrated circuits. *J. Lightwave Technol.* 35(9), 1531–1541 (May 2017)
- Mower, J., et al.: High-fidelity quantum state evolution in imperfect photonic integrated circuits. *Phys. Rev.* 92(3), 032322 (2015)
- Zhu, X., et al.: FPGA controlled microring based tunable add-drop filter. In: 2013 Optical Interconnects Conference, Santa Fe, USA, pp. 102–103 (May 2013)
- Zheng, X., et al.: A high-speed, tunable silicon photonic ring modulator integrated with ultra-efficient active wavelength control. *Optic. Express.* 22(10), 12 628–12 633 (2014)
- Gazman, A., et al.: Automated thermal stabilization of cascaded silicon photonic ring resonators for reconfigurable WDM applications. In: 2017 European Conference on Optical Communication (ECOC), Gothenburg, Sweden, pp. 1–3 (Sep 2017)
- Miller, D.A.B.: Reconfigurable add-drop multiplexer for spatial modes. *Optic. Express.* 21(17), 20 220–20 229 (Aug 2013) .
- Doylend, J., Knights, A.P.: The evolution of silicon photonics as an enabling technology for optical interconnection. *Laser Photon. Rev.* 6(4), 504–525 (2012)
- Li, Y., Poon, A.W.: Active resonance wavelength stabilization for silicon microring resonators with an in-resonator defect-state-absorption-based photodetector. *Optic. Express.* 23(1), 360–372 (Jan 2015)
- Jayatilleka, H., et al.: Photoconductive heaters enable control of large-scale silicon photonic ring resonator circuits. *Optica.* 6(1), 84–91 (2019)
- Gazman, A., et al.: Tapless and topology agnostic calibration solution for silicon photonic switches. *Optic. Express.* 26(25), 32662–32674 (Dec 2018)
- Morichetti, F., et al.: Non-invasive on-chip light observation by contactless waveguide conductivity monitoring. *IEEE J. Sel. Top. Quant. Electron.* 20(4), 292–301 (2014)
- Baehr-Jones, T., Hochberg, M., Scherer, A.: Photodetection in silicon beyond the band edge with surface states. *Optic. Express.* 16(3), 1659–1668 (Feb 2008)
- Zanetto, F., et al.: WDM-Based Silicon Photonic Multi-Socket Interconnect Architecture With Automated Wavelength and Thermal Drift Compensation, In *Journal of Lightwave Technology*, vol. 38, no. 21, pp. 6000–6006, 1 Nov.1, (2020).
- Aguiar, D., et al.: Automatic tuning of silicon photonics microring filter array for hitless reconfigurable add-drop. *J. Lightwave Technol.* 37(16), 3939–3947 (Aug 2019)
- Annoni, A., et al.: Automated routing and control of silicon photonic switch fabrics. *IEEE J. Sel. Top. Quant. Electron.* 22(6), 169–176 (Nov 2016)
- Grillanda, S., et al.: Non-invasive monitoring and control in silicon photonics using CMOS integrated electronics. *Optica.* 1(3), 129–136 (Sep 2014) .
- Padmaraju, K., et al.: Thermal stabilization of a microring modulator using feedback control. *Optic. Express.* 20(27), 27 999–28 008 (Dec 2012) .
- Zortman, W.A., et al.: Bit-error-rate monitoring for active wavelength control of resonant modulators. *IEEE Micro.* 33(1), 42–52 (Jan 2013)
- Padmaraju, K., et al.: Wavelength locking and thermally stabilizing microring resonators using dithering signals. *J. Lightwave Technol.* 32(3), 505–512 (Feb 2014)
- Carminati, M., et al.: Design guidelines for contactless integrated photonic probes in dense photonic circuits. *J. Lightwave Technol.* 35(14), 3042–3049 (2017)
- Milanizadeh, M., et al.: Control and calibration recipes for photonic integrated circuits. *IEEE J. Sel. Top. Quant. Electron.* 26(5), 1–10 (Sept 2020)
- Zhang, Y., et al.: Towards adaptively tuned silicon microring resonators for optical networks-on-chip applications. *IEEE J. Sel. Top. Quant. Electron.* 20(4), 136–149 (July 2014)
- Timurdogan, E., et al.: Automated wavelength recovery for microring resonators. In: 2012 Conference on Lasers and Electro-Optics (CLEO), San Jose, USA, pp. 1–2 (May 2012)
- Milanizadeh, M., et al.: Manipulating free-space optical beams with a silicon photonic mesh. In: 2019 IEEE Photonics Society Summer Topical Meeting Series (SUM), Fort Lauderdale, USA, pp. 1–2 (2019)
- Guglielmi, E., et al.: 16-channel modular platform for automatic control and reconfiguration of complex photonic circuits. In: 2017 IEEE International Symposium on Circuits and Systems (ISCAS), Baltimore, USA, pp. 1–4 (2017)

How to cite this article: Zanetto F, Grimaldi V, Toso F, et al. Dithering-based real-time control of cascaded silicon photonic devices by means of non-invasive detectors. *IET Optoelectron.* 2021;15:111–120. <https://doi.org/10.1049/ote2.12019>